THE JOURNAL OF
PHYSICAL CHEMISTRY C

Article

pubs.acs.org/JPCC

Structures and Phase Transition of a MoS_2 Monolayer

M. Kan,[†] J. Y. Wang,[‡] X. W. Li,[§] S. H. Zhang,[§] Y. W. Li,[†] Y. Kawazoe,[∥] Q. Sun,*[,†,§,⊥] and P. Jena[⊥]

[†]Department of Materials Science and Engineering, [‡]College of Chemistry and Molecular Engineering, and [§]Center for Applied Physics and Technology, Peking University, Beijing 100871, China

[∥]Institute for Material Research, Tohoku University, Sendai 980-8577, Japan

[⊥]Department of Physics, Virginia Commonwealth University, Richmond, Virginia 23284, United States

ABSTRACT: As an inorganic cousin of graphene, MoS_2 monolayer has attracted considerable attention. However, a full understanding of its structure and stability is still lacking due to its dependence on experimental synthesis conditions. Using first-principle calculations combined with Boltzmann transport equation, we have extensively studied the geometry, energetics, electronic structure, optical absorption, and carrier mobility of various phases of MoS_2. We have not only identified the stable phases of a MoS_2 monolayer, but also clarified the specific conditions under which different phases are formed. The possible pathways for transitions among different phases are also discussed.

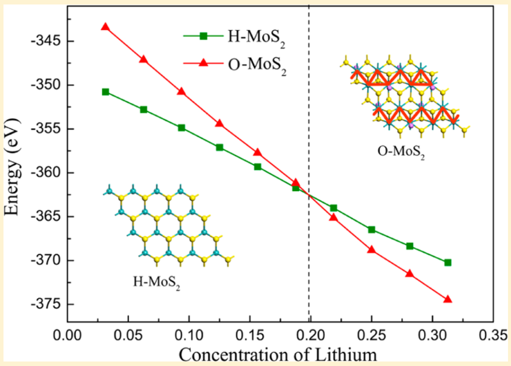

I. INTRODUCTION

The study of two-dimensional (2D) monolayer materials has been a topic of current interest since the first report of the successful fabrication of a 2D single layered graphene by Novoselov et al. in 2004.[1] Among these, molybdenum disulfide (MoS_2) sheet, a transition metal dichalcogenide (TMD), has attracted considerable attention due to its important role in lithium ion battery (LIB),[2] flexible electronic device,[3] photoluminescence,[4] valleytronics,[5,6] and field effect transistors. The technological importance of MoS_2 is further enhanced due to its exceptional properties such as amplification of electrical signals at room temperature with much less power consumption than traditional silicon or even graphene, high room temperature current on/off ratios, ultralow standby power dissipation, and high mobility rate comparable to silicon.[7]

Similar to graphene, monolayer MoS_2 can be extracted from the bulk using mechanical or solvent-based exfoliation method.[7,8] The former method always leads to a 2D trigonal prismatic phase (labeled as H-MoS_2), which is found to be a semiconductor[9] with a direct band gap between the occupied d_{z2} and the empty $d_{x2-y2,xy}$ orbitals. The H-MoS_2 phase has the space group of $P6/mmc$ and is believed to be a stable configuration under normal condition.[10] On the other hand, the solvent-based exfoliation method[11,12] results in different octahedral coordinated phases. The dependence of the structure on experimental synthesis method has been puzzling scientists for a long time. For example, the structure of MoS_2 was originally proposed to be TiS_2 type with nearly ideal octahedral configuration with each Mo atom bonded with six S atoms, which is referred to as T-MoS_2.[13−15] X-ray diffraction study suggested a tetramerization model,[16] while another study[17] showed that the Mo atoms are shifted from their positions to form trigonal clusters in the octahedral MoS_2. The AFM image of a single layer MoS_2 on mica indicated no superlattice formation,[18] while a STM study of the surface layer of restacked MoS_2 indicated a superstructure caused by the formation of zigzag chains.[19] Later, electron crystallography study[12] suggested that the restacked MoS_2 is more like WTe_2 with zigzag Mo−Mo chains rather than that of TiS_2. This is labeled as ZT-MoS_2. Furthermore, Rocquefelte et al.[20] proposed that lithium inserted MoS_2 possesses distorted octahedral coordinated structure with rhombus shape connected Mo−Mo chains, which is referred to as DT-MoS_2. Recently, significant progress has been achieved in the fabrication of MoS_2 nanotubes with octahedral coordination under substitutional rhenium doping.[21] Eda et al.[22] have synthetized a single layer of exfoliated MoS_2 consisting of both trigonal prismatic and octahedral phases with matching lattices so that they form chemically homogeneous atomic and electronic heterostructures with potential for novel molecular functionalities.

From the above, we see that unlike graphene, the structures of MoS_2 monolayer are complicated and confusing. Currently, there is no theoretical study available to clarify the relationships among different structures reported in experiments. This study is aimed at bridging this gap. Our main objective is to understand the specific condition that stabilizes a particular phase and how phase transitions between different phases can be induced. We also study the geometric, electronic, and optical

Received: July 31, 2013
Revised: January 2, 2014

Table 1. Optimized Geometrical Parameters and Energy of H-MoS_2, T-MoS_2, and ZT-MoS_2[a]

	a/Å	b/Å	α/deg	Mo−S/Å	Mo−Mo/Å	E/eV
H-MoS_2	3.19	3.19	120.0	2.41	3.18	0
T-MoS_2	3.19	3.19	120.0	2.43	3.18	0.85
ZT-MoS_2	6.35	6.55	119.0	2.45 (2.39, 2.51)	3.29 (2.77, 3.81)	0.51

[a] For ZT-MoS_2, the Mo−S bond length is in the range of 2.39−2.51 Å with an average length of 2.45 Å. The Mo−Mo bond length is in the range of 2.77−3.81 Å with an average length of 3.29 Å. The relative energy E is given using H-MoS_2 as the reference.

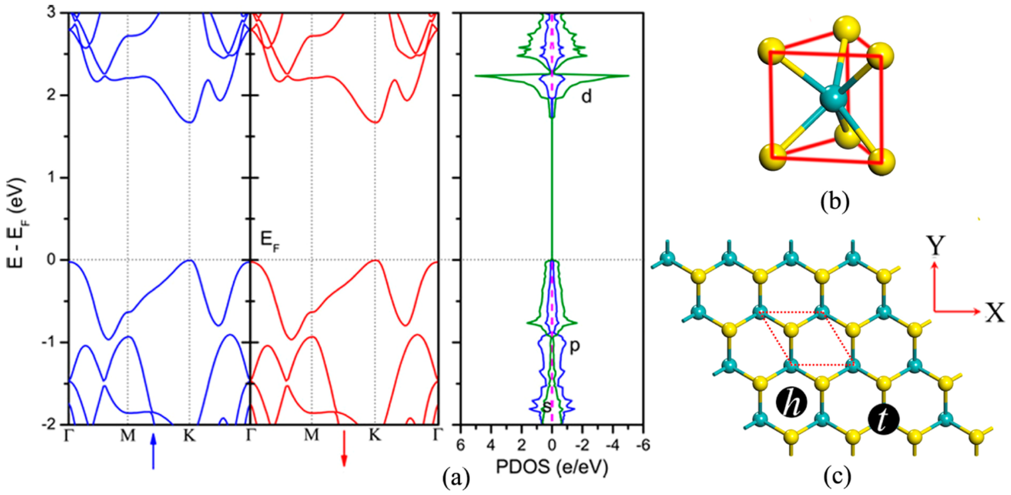

Figure 1. (a) Band structure, PDOS, (b) structural unit, and (c) geometrical structure of trigonal prismatic coordinated (H-MoS_2) 2D MoS_2. (The green and yellow spheres represent the Mo and S atoms, respectively. The two possible Li adsorption sites t and h are denoted in (c).)

properties of different phases. A fundamental understanding of these topics is important to fully harness the technological potential of MoS_2.

Our results based on density functional theory (DFT) calculations show that while a trigonal prismatic H-MoS_2 is the most stable phase, the octahedral coordinated phases can also exist under specific conditions. According to our DFT study and analysis, ZT-MoS_2, which is a charge density wave (CDW) state, can be stable at low temperature. When ZT-MoS_2 gains some energy from the outside, the CDW state becomes unstable turning to an undistorted octahedral coordinated phase (T-MoS_2) without Mo−Mo clustering. Moreover, lithium adsorption and electron charging can stabilize another octahedral coordinated structure (DT-MoS_2). We find that the trigonal prismatic H-MoS_2 is a direct semiconductor with a band gap of 1.67 eV, and the ZT-MoS_2 has a much smaller band gap of 0.022 eV. T-MoS_2, on the other hand, is metallic. Our results suggest that due to much higher carrier mobility, ZT-MoS_2 may have a greater potential over H-MoS_2 as a promising material for microelectronics. The calculated optical properties of H-MoS_2 and ZT-MoS_2 show that they have different optical features. Furthermore, Li adsorption on the surface can induce a phase transition from H-MoS_2 to an octahedral coordinated MoS_2. We find that charging the 2D MoS_2 with electrons can reverse the phase stabilities, which is another strategy to induce a phase transition. We also discuss the entire reversible recycling process of the phase transition induced by Li adsorption with detailed evolution of the structures. This will be helpful to better understand the basic processes involved in MoS_2-based LIB.

II. COMPUTATIONAL METHODS

Our calculations are based on spin-polarized density functional theory (DFT) with the Perdew−Burke−Ernzerhof (PBE) form for the generalized gradient approximation (GGA)[23] to the exchange-correlation potential. All calculations are performed using Vienna ab initio simulation package (VASP) code,[24] ultrasoft pseudopotentials, and a plane-wave basis set with the projector augmented plane-wave method (PAW).[25] The periodic boundary condition is used to simulate 2D monolayer MoS_2, and all of the structures are relaxed without any symmetry constraint. We use a vacuum space of 25 Å in the periodic directions to avoid interactions between two neighboring images. The reciprocal space is represented by Monkhorst−Pack special k-point scheme[26] with 19 × 19 × 1, 11 × 11 × 1, and 5 × 5 × 1 grid meshes for the (1 × 1) unit cell, the (2 × 2), and (4 × 4) supercell, respectively. The criteria of convergence for energy and force, as well as energy cutoff, are set to be 1×10^{-4} eV, 0.01 eV/Å, and 360 eV, respectively. In addition, for comparison, the state-of-the-art hybrid functional (HSE06)[27,28] is carried out to study the electronic properties. For the optical spectra, the imaginary part of dielectric function is determined by a summation over empty states in the whole Brillouin zone.[29]

III. RESULTS AND DISCUSSION

III.1. Phase Stability of 2D Monolayer MoS_2. To test the accuracy of our method, we first calculate the trigonal prismatic phase (H-MoS_2) with GGA-PBE by using a 1 × 1 unit cell. The optimized geometrical parameters are given in Table 1. Our calculated results show that the optimized bond distance between Mo and S atoms d_{Mo-S} = 2.41 Å, the distance between two S atoms at each corner d_{S-S} = 3.13 Å, and the angle between Mo−S bonds θ_{S-Mo-S} = 80.73°. These agree well with the results of Ciraci et al.,[30] 2.42 Å, 3.13 Å, and 80.69°, respectively. A monolayer H-MoS_2 is a nonmagnetic semiconductor possessing a direct band gap with the valence band maximum (VBM) and conduction band minimum (CBM) situated at the K point of the Brillouin zone. The calculated energy gap of H-MoS_2, 1.67 eV, agrees well with previous theoretical result with GGA-PBE.[31,32] We also calculated the energy band structure using the HSE06 functional, and the energy gap is calculated to be 2.13 eV in agreement with the previous study.[30] To get a precise description of the optical band gap of monolayer MoS_2, one may need to consider GW and Bethe−Salpeter calculation methods.[33−36] However, due to the limited computational resources, we use the PBE method for the qualitative understanding of the optical properties.

Figure 2 presents the other three possible metastable configurations of MoS_2 single layer synthesized using the chemical solvent-based exfoliation methods.[12,13,20] These can be classified into three groups: octahedral coordinated MoS_2, referred to as T-MoS_2 (Figure 2b); distorted octahedral coordinated MoS_2 with zigzag Mo−Mo chains, referred to as ZT-MoS_2 (Figure 2c); and distorted octahedral coordinated MoS_2 in rhombus-shape with Mo−Mo chains, referred to as DT-MoS_2 (Figure 2d). For convenience, we use O-MoS_2 to describe all three octahedral coordinated MoS_2 regardless of the detail of the molybdenum clusterization.

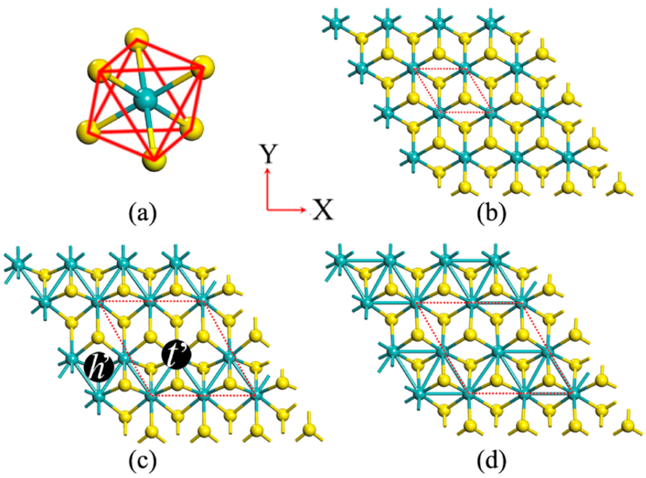

Figure 2. (a) Structural unit of octahedral coordinated 2D MoS_2. Geometric structures of (b) T-MoS_2, (c) ZT-MoS_2, and (d) DT-MoS_2. (The two possible Li adsorption sites t' and h' are denoted in (c).)

For the calculations of geometric and electronic properties as well as phase stability, we use (1 × 1), (2 × 2), and (2 × 2) super cells for T-MoS_2, ZT-MoS_2, and DT-MoS_2, respectively. It should be noted here that the ZT-MoS_2 phase is the same phase named T-phase in Eda et al.'s work.[22] We first discuss the results of T-MoS_2 and ZT-MoS_2. The (1 × 1) T-MoS_2 and the (2 × 2) ZT-MoS_2 maintain their structures after relaxation. However, we observed a structural transition to ZT-MoS_2 after the (1 × 1) cell of T-MoS_2 is increased to (2 × 2) and (4 × 4). In other words, free-standing T-MoS_2 is unstable at 0 K. The structural transition from T-MoS_2 to ZT-MoS_2, which is a charge density wave (CDW) state,[37,38] is due to the Peierls instability. Below the critical Peierls transition temperature (T_p), the elastic energy cost to modulate the atomic positions in T-MoS_2 to ZT-MoS_2 is less than the gain in electronic energy. Thus, the lattice of atoms undergoes a periodic distortion, and the electrons condense into a collective state with a periodic modulation of the charge density leading to the CDW state. This is known as Peierls' transition.[39] Because the Mo atom in the octahedral coordinated position has a d^2 configuration, each Mo uses only two of the three in-plane t_{2g} orbitals. This fits the two-center, two-electron bonding model, which requires each Mo atom to bind with two neighboring Mo atoms to form two bonds as shown in Figure 2c. This results in a relatively stable zigzag chain configuration. In addition, an earlier experimental study[4] showed that the octahedral-based phase (O-MoS_2) will transform to H-MoS_2 if the annealing temperature reaches to a critical temperature T_t (∼300 °C). As for DT-MoS_2, our results show that the (2 × 2) structure is also unstable and transforms to the ZT-MoS_2 spontaneously. Although the pure free-standing DT-MoS_2 is not stable, it can exist in some impure state through the lithium adsorption or charging as shown in section III.3.

Numerically, the optimized ZT-MoS_2 is more stable than the undistorted T-MoS_2 by 0.34 eV in total energy. It is higher than that of H-MoS_2 by 0.51 eV for a unit cell as listed in Table 1. The fully relaxed lattice parameters and interatomic distances are also given in Table 1. The cell parameter "a" for ZT-MoS_2 undergoes about 0.3% contraction, while "b" undergoes about 2.8% expansion as compared to that of H-MoS_2. No significant deviation from 120° is found for the "α" (=119.0°) angle. The Mo−S and Mo−Mo bond lengths (2.45 and 3.29 Å on average) are elongated for the ZT-MoS_2 as compared to H-MoS_2. We obtain a shorter Mo−Mo distance of 2.77 Å inside

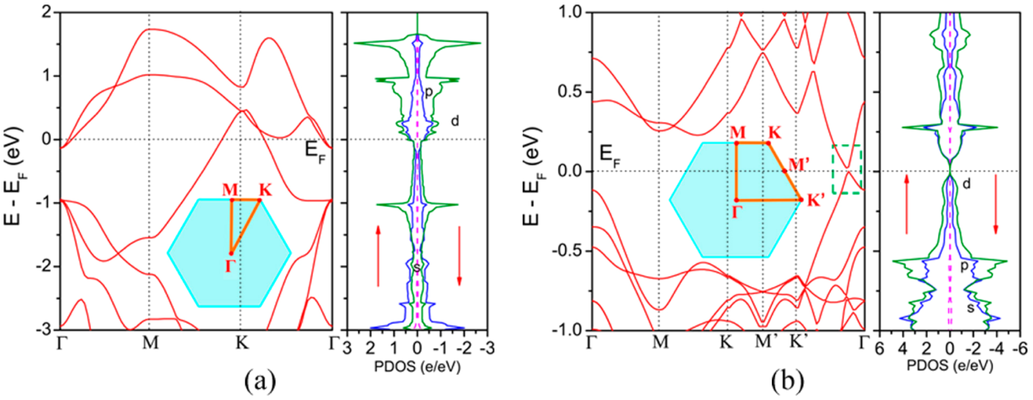

Figure 3. Band structures and PDOS of the optimized (a) (1 × 1) T-MoS_2 and (b) (2 × 2) ZT-MoS_2 along the lines connecting high-symmetry points of the Brillouin zone.

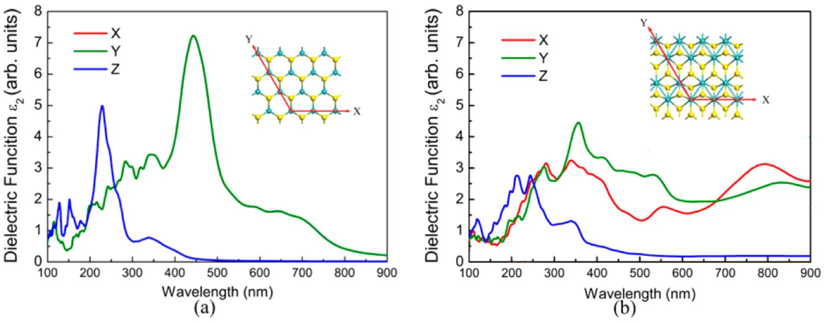

Figure 4. Calculated imaginary part of the dielectric function for parallel (X, Y) and perpendicular (Z) polarization of (a) monolayer H-MoS_2 and (b) ZT-MoS_2.

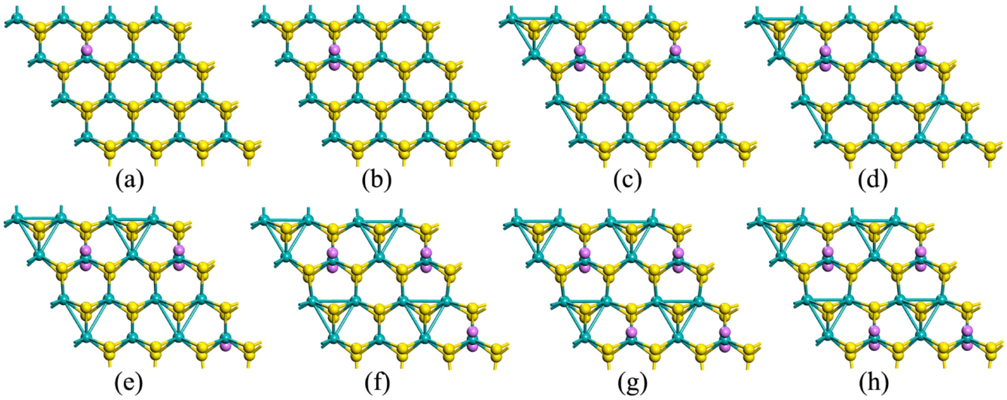

Figure 5. The optimized structures of the most stable Li@H-MoS_2 with 1−8 Li atoms.

the cluster and a longer distance of 3.81 Å between the clusters, which results from the CDW.

III.2. Electronic and Optical Properties of MoS_2 Monolayer. The electronic properties of pure 2D MoS_2 are studied in detail below. The band structures calculated by GGA-PBE for a monolayer of T-MoS_2 and ZT-MoS_2 along the lines connecting the high-symmetry points of the Brillouin zone are shown in Figure 3. We have carried out spin-polarized calculations to see if the ground state could be magnetic, but two-dimensional T-MoS_2 and ZT-MoS_2 remain nonmagnetic. The structural distortions of monolayer dichalcogenides ZT-MoS_2 lead to the opening of a direct gap of 0.022 eV in the electronic structure as compared to the undistorted metallic T-MoS_2 as shown in Figure 3b. Additionally, the band gap of ZT-MoS_2 is calculated to be 0.23 eV, and T-MoS_2 is still metallic with HSE06. In the following, we calculate the carrier mobility and optical properties of 2D H-MoS_2 and ZT-MoS_2. T-MoS_2 is not considered because it is metallic as shown in Figure 3a.

To further explore the potential applications of the less studied 2D ZT-MoS_2, we use density functional theory coupled with Boltzmann transport equation[40] to investigate the acoustic phonon-dominated mobility[41] of ZT-MoS_2 and H-MoS_2 at temperature $T = 100$ K. Two transporting directions labeled as X and Y (Figures 1 and 2) were considered. The intrinsic electron density is estimated to be 1×10^{10} cm^{-2}, which is much lower than that of n-doped H-MoS_2 used in the experiment.[7] The calculated electron (hole) mobility of H-MoS_2 is 1.2 (3.8) × 10^2 cm^2 V^{-1} s^{-1} along both X and Y directions. These results fit well with the theoretical predictions when the dependence of mobility on carrier density and temperature is considered.[42,43] Interestingly, ZT-MoS_2 has electron and hole mobility 1 (2) order(s) of magnitude higher than that of H-MoS_2 along the X (Y) direction. More specifically, the electron (hole) mobility of ZT-MoS_2 is 4.1 (2.1) × 10^3 and 6.4 (5.7) × 10^4 cm^2 V^{-1} s^{-1} along the X and Y directions, respectively. The great improvement in the mobility can be attributed to the reduction of electron (hole) effective mass[44] from 0.49 (0.60) m_e to 0.12 (0.05) m_e when H-MoS_2 is transformed to ZT-MoS_2. In particular, the mobility of ZT-MoS_2 is higher than that of silicon and comparable to that of graphene nanoribbons and graphene transistors.[45−47] Up to now, only 2D monolayer H-MoS_2 has been studied experimentally for application in electronic devices. According to the high carrier mobility of ZT-MoS_2, it is reasonable to believe that the ZT-MoS_2 would have extensive potential applications in electronic devices.

Because of the strong photoluminescence of monolayer H-MoS_2,[48] we have studied the optical properties of both phases. The PBE-calculated imaginary parts of the dielectric functions for monolayer H-MoS_2 and ZT-MoS_2 are shown in Figure 4. The calculation details can be found in a previous study.[49] We see that our results for monolayer H-MoS_2 can accurately reproduce the experimentally observed optical absorption spectrum.[4] Our calculations show a sharp absorption peak around 450 nm and another lower peak at 230 nm, which fits the experimental results of Eda et al.[4] very well. The absorption of ZT-MoS_2 covers a wider range than that of H-MoS_2, although there are no sharp absorption peaks. For in-plane polarization, ZT-MoS_2 monolayer is optically anisotropic, which is different from the H-MoS_2 monolayer because of their different lattice structure. Thus, our calculated results indicate that the two different MoS_2 monolayer phases may have different optical applications. Additionally, the absorption

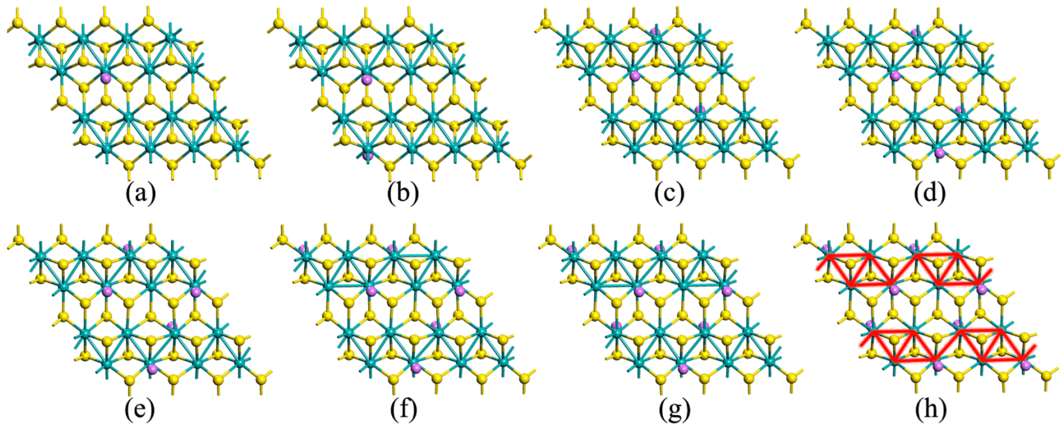

Figure 6. The optimized structures of the most stable Li@ZT-MoS_2 with 1−8 Li atoms. Mo atoms form a diamond-like chain in (h) as highlighted in red.

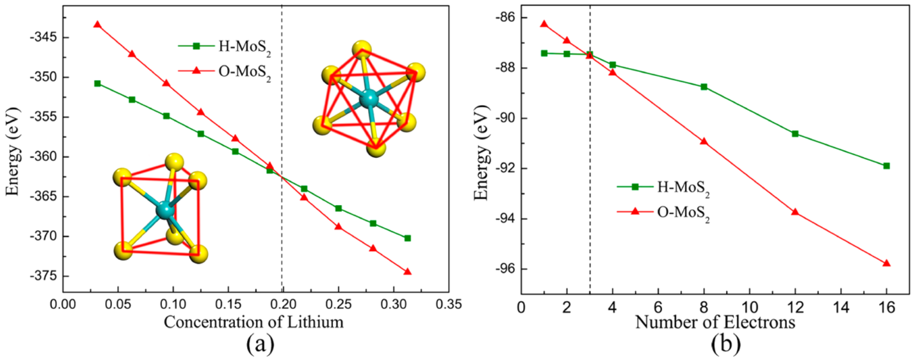

Figure 7. (a) Variation of the energy for H-MoS_2 and O-MoS_2 as the concentration of Li changes. (b) The variation of the energy for H-MoS_2 and O-MoS_2 with respect to the number of electrons in the systems.

spectra of different phases provide an efficient method to identify them experimentally.

III.3. Phase Transition of 2D MoS_2 Monolayer Induced by Lithium Insertion. In recent years, 2D MoS_2 has attracted much attention as electrode material for LIB due to its high surface area and short diffusion length.[2,50] In the following, we introduce lithium atoms on the surface of 2D MoS_2 to induce phase transition, which is a typical procedure for both the discharge/charge processes in LIB and the solvent-based exfoliation of MoS_2 monolayer. As far as we know, no experimental or theoretical studies have been reported in detail on the phase transition process.

First, we check the stable lithium adsorption sites on 2D H-MoS_2 and ZT-MoS_2 as illustrated in Figures 5a and 6a. For H-MoS_2, two possible sites are examined as shown in Figure 1: (1) top of Mo atom (t) sites; and (2) hollow (h) sites above the center of hexagon. For ZT-MoS_2, two other possible sites are also considered as shown in Figure 2: (1) top of Mo atom (t') sites; and (2) hollow (h') sites above the center of S−S triangle but not on top of a Mo atom. It should be pointed out that the Li atoms move from the t' sites slightly after relaxation in ZT-MoS_2, while they stay above the t sites in H-MoS_2. To represent the stability of the Li adsorbed system, we calculate the binding energy (E_b), which is defined as $E_b = E_{Li@MoS2} - nE_{Li} - E_{MoS2}$. n indicates the number of Li atoms, while $E_{Li@MoS2}$, E_{Li}, and E_{MoS2} indicate the energies of Li adsorbed MoS_2, Li atom, and MoS_2 monolayer, respectively. The calculated binding energy shows that a Li atom on t site is about 0.15 eV lower than that on h site for H-MoS_2, while it is energetically degenerate for a Li atom to occupy t' and h' sites in ZT-MoS_2. Nevertheless, we still consider h and h' sites for inserting additional Li atoms in the following. All possible Li distributions are considered in our calculations keeping symmetry in mind. Once the Li site distribution with the lowest energy has been found, we choose this as well as the second lowest energy configuration as two initial structures for introducing another Li atom. This process is repeated until the number of Li atoms increases to 10 in a (4 × 4) supercell.

We extensively examined the most stable configurations of Li@MoS_2. These are shown in Figures 5 and 6 for 1−8 Li atoms. As more Li atoms are added to the surface, clustering of Mo increases in both phases. Comparing the possible sites of t, t', h, and h', we found that Li atoms prefer to reside on t and t' sites for all concentrations. Figure 7a gives the variation of the energies for both Li@H-MoS_2 and Li@ZT-MoS_2 as the concentration of Li increases. Because there are 32 most stable sites for Li atoms on (4 × 4) supercell of 2D MoS_2, the concentration of Li is defined as the number of Li atoms n divided by 32 (n/32 × 100%). As shown in Figure 5a, the H-MoS_2 is still the most stable phase when 1−6 Li atoms are added to the system. When the concentration of Li atoms exceeds 20%, O-MoS_2 becomes more stable, which means that the phase transition in 1 kg of 2D H-MoS_2 can be induced with only 17.5 g of Li. Before the transition point, some triangular Mo−Mo clustering appears in Li@H-MoS_2, while after the transition point the state of the Mo−Mo clustering in 7Li@O-MoS_2 is between ZT-MoS_2 and DT-MoS_2. When 8 Li atoms are introduced, Mo atoms form a diamond-like chain as shown in Figure 6h. As we continue introducing up to 10 Li atoms, the system can maintain the "diamond chain" structure. We subsequently checked the structure of O-MoS_2 with 100% Li concentration, which shows that the DT-MoS_2 configuration is still stable. The transformation of the Mo−Mo clustering from zigzag chain to diamond chain can also be understood by analyzing the valence electronic configuration. As Li atoms are added on the surface of MoS_2, electrons transfer from Li atoms to the host. In other words, the valence electron configuration of Mo atoms in the octahedral coordination will undergo a transformation from d^2 to d^3. Thus, the t_{2g} levels of each Mo atom can accommodate one electron per level, and each Mo atom will need to form two-center two-electron σ-bonds with the three neighboring Mo atoms,[38] resulting in the diamond-chain configuration. We believe that the transition from trigonal prismatic coordination to octahedral coordination is also caused by the transfer of electrons from Li atoms to the MoS_2 sheet. From the band structure of H-MoS_2 and ZT-MoS_2, it can be seen that the conduction band of H-MoS_2 is much higher above the Fermi level as compared to that of ZT-MoS_2. Thus, the introduced electrons in H-MoS_2 will increase the energy of H-MoS_2 by a higher level than that of ZT-MoS_2. To verify this conjecture, we charged the (2×2) supercell of H-MoS_2 and O-MoS_2 with electrons, and the results are shown in Figure 7b. Note that O-MoS_2 becomes more stable than the H-MoS_2 as the number of electrons increases. The DT-MoS_2 configuration is formed after charging. This is similar to what we observed with Li doping. Only 3 electrons can induce a (2×2) supercell to undergo phase transition, corresponding to -8.33×10^{14} cm^{-2}. We further check the dependence of the results on the supercell size in the transverse direction. Our result shows that the phase transition occurs when 14 electrons are injected in a $4 \times 4 \times 1$ supercell with the charge density of -9.71×10^{14} cm^{-2}. The required concentrations for inducing the phase transition are quite similar for the two supercells. We also confirmed Kertesz−Hoffmann's theory that a d^2 to d^3 transformation can sometimes induce a transfer from trigonal prismatic coordination to octahedral coordination.

It is important to note that in an earlier experimental study,[12] S atoms in 2D MoS_2 were found to keep the octahedral coordination after all of the Li atoms were removed, but the detailed structural information was lacking. On the basis of our study, we conclude that this kind of octahedral coordinated configuration without Li atoms is possible for the ZT-MoS_2 phase, which is metastable and can transform to H-MoS_2 after heating or aging.[4] Combining these experimental works with our theoretical calculation, we summarize the possible pathways for structural phase transition among different structures in Figure 8: H-MoS_2 → O-MoS_2→ DT-MoS_2→ ZT-MoS_2 → H-MoS_2. The detailed process is the following: (1) When Li atoms are introduced to H-MoS_2, the trigonal prismatic H-MoS_2 remains stable until the Li concentration reaches 20%. (2) When more Li atoms are inserted, the octahedral coordinated O-MoS_2 becomes more stable. The structure transforms from zigzag chains to "diamond chains" and finally forms the stable DT-MoS_2 phase. (3) When all of the Li atoms are extracted from the system, the structure becomes ZT-MoS_2. (4) Through heating or aging, the ZT-MoS_2 will transform back to the most stable phase H-MoS_2. We hope that the pathways discussed above will help experimentalists to better understand the detailed process involved in MoS_2-based LIB and in the liquid phase exfoliation of monolayer MoS_2 through Li intercalation.

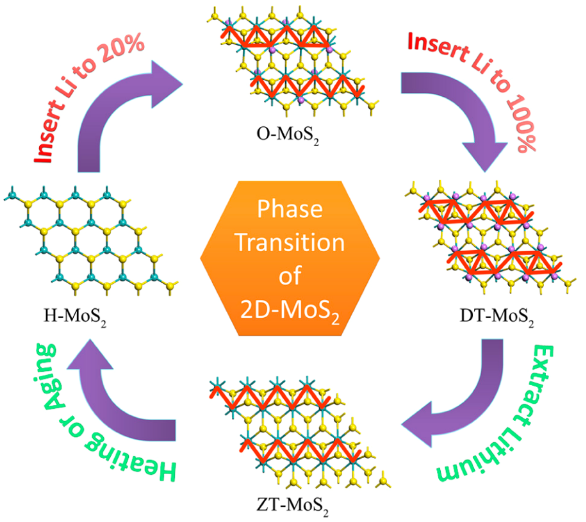

Figure 8. Possible pathways of structural phase transition in MoS_2 monolayer.

IV. SUMMARY

A comprehensive study of the relative phase stability of MoS_2 monolayer led us to the following conclusions: (1) Two phases were identified that can be stable under normal conditions, the traditional trigonal prismatic H-MoS_2 phase and the distorted octahedral ZT-MoS_2 phase with zigzag Mo−Mo chains. (2) Li insertion with concentration of 20% or electron charging with concentration of 8.33×10^{14} cm^{-2} can induce structural transitions. (3) MoS_2 monolayer not only displays complicated geometries but also exhibits rich physical properties: H-MoS_2 is a semiconductor with a direct band gap of 1.67 eV. ZT-MoS_2 is also a direct band gap semiconductor, but with a much smaller band gap of 0.022 eV. T-MoS_2, on the other hand, is metallic. Furthermore, the electron (hole) mobility of ZT-MoS_2 is found to be 4.1 (2.1) $\times 10^3$ and 6.4 (5.7) $\times 10^4$ $cm^2\ V^{-1}\ s^{-1}$ along the X and Y directions, respectively, which are much higher than the corresponding values of 1.2 (3.8) $\times 10^2$ $cm^2\ V^{-1}\ s^{-1}$ in H-MoS_2. (4) H-MoS_2 and ZT-MoS_2 show very different optical properties, which can be used to identify their structures. (5) DT-MoS_2 can be formed with lithium adsorptions or electron injections; when the lithium atoms on the surface are removed, the ZT-MoS_2 phase then forms. It is hoped that the information provided in this study will help experimentalists to better understand the geometries and properties of MoS_2 monolayers.

■ AUTHOR INFORMATION

Corresponding Author

*E-mail: sunqiang@pku.edu.cn.

Notes

The authors declare no competing financial interest.

■ ACKNOWLEDGMENTS

This work is partially supported by grants from the National Natural Science Foundation of China (NSFC-21173007, 11274023), the National Grand Fundamental Research 973 Program of China (2012CB921404), the U.S. Department of Energy, Office of Basic Energy Sciences, Division of Materials Sciences and Engineering under Award no. DE-FG02-96ER45579, and JST, CREST, "A mathematical challenge to a new phase of material sciences" (2008−2013). We thank

Prof. Zhigang Shuai for help with mobility calculations and the crew of the Center for Computational Materials Science, the Institute for Materials Research, Tohoku University (Japan), for their continuous support of the HITACHSR11000 supercomputing facility.

■ REFERENCES

(1) Novoselov, K. S.; Geim, A. K.; Morozov, S. V.; Jiang, D.; Zhang, Y.; Dubonos, S. V.; Grigorieva, I. V.; Filrsov, A. A. Electric Field Effect in Atomically Thin Carbon Films. *Science* **2004**, *306*, 666−669.

(2) Hwang, H.; Kim, H.; Cho, J. MoS_2 Nanoplates Consisting of Disordered Graphene-Like Layers for High Rate Lithium Battery Anode Materials. *Nano Lett.* **2011**, *11*, 4826−4830.

(3) Bertolazzi, S.; Brivio, J.; Kis, A. Stretching and Breaking of Ultrathin MoS_2. *ACS Nano* **2011**, *5*, 9703−9709.

(4) Eda, G.; Yamaguchi, H.; Voiry, D.; Fujita, T.; Chen, M.; Chhowalla, M. Photoluminescence from Chemically Exfoliated MoS_2. *Nano Lett.* **2012**, *11*, 5111−5116.

(5) Cao, T.; Wang, G.; Han, W.; Ye, H.; Zhu, C.; Shi, J.; Niu, Q.; Tan, P.; Wang, E.; Liu, B.; Feng, J. Valley-Selective Circular Dichroism of Monolayer Molybdenum Disulphide. *Nat. Commun.* **2012**, *3*, 887−892.

(6) Mak, K.; He, K.; Shan, J.; Heinz, T. F. Control of Valley Polarization in Monolayer MoS_2 by Optical Helicity. *Nat. Nanotechnol.* **2012**, *7*, 494−498.

(7) Radisavljevic, B.; Radenovic, A.; Brivio1, J.; Giacometti, V.; Kis, A. Single-layer MoS_2 Transistors. *Nat. Nanotechnol.* **2011**, *6*, 147−150.

(8) Lee, C.; Li, Q. Y.; Kalb, W.; Liu, X. Z.; Berger, H.; Carpick, R. W.; Hone, J. Frictional Characteristics of Atomically Thin Sheets. *Science* **2010**, *328*, 76−80.

(9) Qin, X. R.; Yang, D.; Frindt, R. F.; Irwin, J. C. Real-Space Imaging of Single-Layer MoS_2 by Scanning Tunneling Microscopy. *Phys. Rev. B* **1991**, *44*, 3490−3493.

(10) Benavente, E.; Santa Ana, M. A.; Mendizabal, F.; Gonzalez, G. Intercalation Chemistry of Molybdenum Disulfide. *Coord. Chem. Rev.* **2002**, *224*, 87−109.

(11) Gordon, R. A.; Yang, D.; Crozier, E. D.; Jiang, D. T.; Frindt, R. F. Structures of Exfoliated Single Layers of WS_2, MoS_2, and $MoSe_2$ in Aqueous Suspension. *Phys. Rev. B* **2002**, *65*, 125407−125416.

(12) Heising, J.; Kanatzidis, M. G. Structure of Restacked MoS_2 and WS_2 Elucidated by Electron Crystallography. *J. Am. Chem. Soc.* **1999**, *121*, 638−643.

(13) Py, M. A.; Haering, R. R. Structural Destabilization Induced by Lithium Intercalation in MoS_2 and Related Compounds. *Can. J. Phys.* **1983**, *61*, 76−84.

(14) Chianelli, R. R.; Scanlon, J. C.; Thompson, A. H. Structure Refinement of Stoichiometric TiS_2. *Mater. Res. Bull.* **1975**, *10*, 1379−1382.

(15) Ataca, C.; Şahin, H.; Ciraci, S. Stable, Single-Layer MX_2 Transition-Metal Oxides and Dichalcogenides in a Honeycomb-Like Structure. *J. Phys. Chem. C* **2012**, *116*, 8983−8999.

(16) Yang, D.; Sandovals, S. J.; Divigalpitiya, W. M. R.; Irwin, J. C.; Frindt, R. F. Structure of Single-Molecular-Layer MoS_2. *Phys. Rev. B* **1991**, *43*, 12053−12056.

(17) Wypych, F.; Weber, Th.; Prins, R. Scanning Tunneling Microscopic Investigation of 1T-MoS_2. *Chem. Mater.* **1998**, *10*, 723−727.

(18) Schumacher, A.; Scandella, L.; Kruse, N.; Prins, R. Single-Layer MoS_2 on Mica: Studies by Means of Scanning Force Microscopy. *Surf. Sci. Lett.* **1993**, *289*, L595−L598.

(19) Qin, X. R.; Yang, D.; Frindt, R. F.; Irwin, J. C. Scanning Tunneling Microscopy of Single-Layer MoS_2 in Water and Butanol. *Ultramicroscopy* **1992**, *42*, 630−636.

(20) Rocquefelte, X.; Boucher, F.; Gressier, P.; Ouvrard, G. Mo Cluster Formation in the Intercalation Compound $LiMoS_2$. *Phys. Rev. B* **2000**, *62*, 2397−2400.

(21) Andrey, N. E.; Lena, Y.; Lothar, H.; Igor, P.; Marc, W.; Reshef, T.; Maya, B. S.; Gotthard, S. New Route for Stabilization of 1T-WS_2 and MoS_2 Phases. *J. Phys. Chem. C* **2011**, *115*, 24586−24591.

(22) Eda, G.; Fujita, T.; Yamaguchi, H.; Voiry, D.; Chen, M.; Chhowalla, M. Coherent Atomic and Electronic Heterostructures of Single-Layer MoS_2. *ACS Nano* **2012**, *6*, 7311−7317.

(23) Perdew, J. P.; Burke, K.; Ernzerhof, M. Generalized Gradient Approximation Made Simple. *Phys. Rev. Lett.* **1996**, *77*, 3865−3868.

(24) Kresse, G.; Furthmuller, J. Efficient Iterative Schemes for ab initio Total-Energy Calculations using a Plane-Wave Basis Set. *Phys. Rev. B* **1996**, *54*, 11169−11186.

(25) Kresse, G.; Joubert, D. From Ultrasoft Pseudopotentials to the Projector Augmented-Wave Method. *Phys. Rev. B* **1999**, *59*, 1758−1775.

(26) Monkhorst, H. J.; Pack, J. D. Special Points for Brillouin-Zone Integrations. *Phys. Rev. B* **1976**, *13*, 5188−5192.

(27) Heyd, J.; Scuseria, G. E.; Ernzerhof, M. Hybrid Functionals Based on A Screened Coulomb Potential. *J. Chem. Phys.* **2003**, *118*, 8207−8215.

(28) Heyd, J.; Scuseria, G. E.; Ernzerhof, M. Erratum: "Hybrid Functionals Based on A Screened Coulomb Potential. *J. Chem. Phys.* **2006**, *124*, 219906.

(29) Gajdoš, M.; Hummer, K.; Kresse, G.; Furthmüller, J.; Bechstedt, F. Linear Optical Properties in the Projector-Augmented Wave Methodology. *Phys. Rev. B* **2006**, *73*, 045112−045120.

(30) Ataca, C.; S-ahin, H.; Akturk, E.; Ciraci, S. Mechanical and Electronic Properties of MoS_2 Nanoribbons and Their Defect. *J. Phys. Chem. C* **2011**, *115*, 3934−3941.

(31) Johari, P.; Shenoy, V. B. Tuning the Electronic Properties of Semiconducting Transition Metal Dichalcogenides by Applying Mechanical Strains. *ACS Nano* **2012**, *6*, 5449−5456.

(32) Ding, Y.; Wang, Y.; Ni, J.; Shi, L.; Shi, S.; Tang, W. First Principles Study of Structural, Vibrational and Electronic Properties of Graphene-Like MX_2 (M=Mo, Nb, W, Ta; X=S, Se, Te) Monolayers. *Physica B: Condens. Matter* **2011**, *406*, 2254−2260.

(33) Cheiwchanchamnangij, T.; Lambrecht, W. R. L. Quasiparticle Band Structure Calculation of Monolayer, Bilayer, and Bulk MoS_2. *Phys. Rev. B* **2012**, *85*, 205302−205305.

(34) Komsa, H. P.; Krasheninnikov, A. V. Effects of Confinement and Environment on The Electronic Structure and Exciton Binding Energy of MoS_2 from First Principles. *Phys. Rev. B* **2012**, *86*, 241201−241206.

(35) Shi, H.; Pan, H.; Zhang, Y.; Yakobson, B. I. Quasiparticle Band Structures and Optical Properties of Strained Monolayer MoS_2 and WS_2. *Phys. Rev. B* **2013**, *87*, 155304−155311.

(36) Molina-Ŝanchez, A.; Sangalli, D.; Hummer, K.; Marini, A.; Wirtz, L. Effect of Spin-Orbit Interaction on The Optical Spectra of Single-layer, Double-layer, and Bulk MoS_2. *Phys. Rev. B* **2013**, *88*, 045412−045417.

(37) Kertesz, M.; Hoffmann, R. Octahedral vs. Trigonal-Prismatic Coordination and Clustering in Transition-Metal Dichalcogenides. *J. Am. Chem. Soc.* **1984**, *106*, 3453−3460.

(38) Whangbo, M.; Canadell, E. Analogies Between the Concepts of Molecular Chemistry and Solid-State Physics Concerning Structural Instabilities. Electronic Origin of The Structural Modulations in Layered Transition Metal Dichalcogenides. *J. Am. Chem. Soc.* **1992**, *114*, 9587−9600.

(39) Perierls, R. E. Zur Theorie der Elektrischen und Thermischen Leitfähigkeit von Metallen. *Ann. Phys. (Leipzig, Ger.)* **1930**, *4*, 121−148.

(40) Kaasbjerg, K.; Thygesen, K. S.; Jacobsen, K. W. Phonon-Limited Mobility in n-Type Single-Layer MoS_2 from First Principles. *Phys. Rev. B* **2012**, *85*, 115317−115322.

(41) Shuai, Z. G.; Long, M. Q.; Tang, L.; Wang, D.; Li, Y. L. Electronic Structure and Carrier Mobility in Graphdiyne Sheet and Nanoribbons: Theoretical Predictions. *ACS Nano* **2011**, *5*, 2593−2600.

(42) Kaasbjerg, K.; Jauho, A. P.; Thygesen, K. S. Acoustic Phonon-Limited Mobility in Two-Dimensional MoS_2: Deformation Potential

and Piezoelectric Scattering from First Principles. *Phys. Rev. B* **2013**, *87*, 235312−235326.

(43) Fivaz, R.; Mooser, E. Mobility of Charge Carriers in Semiconducting Layer Structures. *Phys. Rev.* **1967**, *163*, 743−755.

(44) Bruzzone, S.; Fiori, G. Ab-initio Simulations of Deformation Potentials and Electron Mobility in Chemically Modified Graphene and Two-Dimensional Hexagonal Boron-Nitride. *Appl. Phys. Lett.* **2011**, *99*, 222108−222110.

(45) Long, M. Q.; Tang, L.; Wang, D.; Wang, J.; Shuai, Z. G. Theoretical Predictions of Size-Dependent Carrier Mobility and Polarity in Graphene. *J. Am. Chem. Soc.* **2009**, *131*, 17728−17729.

(46) Canali, C.; Jacoboni, C.; Nava, F.; Ottaviani, G.; Alberigi-Quaranta, A. Electron Drift Velocity in Silicon. *Phys. Rev. B* **1975**, *12*, 2265−2284.

(47) Ottaviani, G.; Reggiani, L.; Canali, C.; Nava, F.; Alberigi-Quaranta, A. Hole Drift Velocity in Silicon. *Phys. Rev. B* **1975**, *12*, 3318−3329.

(48) Cheiwchanchamnangij, T.; Lambrecht, W. R. L. Quasiparticle Band Structure Calculation of Monolayer, Bilayer, and Bulk MoS_2. *Phys. Rev. B* **2012**, *85*, 205302−205305.

(49) Li, X.; Zhang, S.; Wang, Q. Stability and Physical Properties of A Tri-Ring Based Porous g-C_4N_3 Sheet. *Phys. Chem. Chem. Phys.* **2013**, *15*, 7142−7146.

(50) Chang, K.; Chen, W. L-Cysteine-Assisted Synthesis of Layered MoS_2/Graphene Composites with Excellent Electrochemical Performances for Lithium Ion Batteries. *ACS Nano* **2011**, *5*, 4720−4728.